Malaysian Journal of Mathematical Sciences 20(2): 739–761 (2026)
https://doi.org/10.47836/mjms.20.2.15

Malaysian Journal of Mathematical Sciences

Journal homepage: https://mjms.upm.edu.my

Effect of MHD on Dusty Mixed Convection Heat Transfer Past a Sphere in Newtonian Fluid

Jefri N. N. N. [1] and Ali A.*[1]

[1]*Department of Mathematical Sciences, Faculty of Science, Universiti Teknologi Malaysia, 81310 Skudai, Johor, Malaysia*

E-mail: anati@utm.my
**Corresponding author*

Received: 11 April 2025
Accepted: 9 November 2025

Abstract

This study presents a mathematical model for unsteady magnetohydrodynamics (MHD) fluid flow past a sphere, incorporating mixed convective heat transfer and suspended dust particles. The existence of dust particles significantly alters flow properties, influencing velocity, temperature distribution, and boundary layer behavior. The governing equations for fluid and dust phases are solved numerically using the Keller-box method implemented in MATLAB. The results demonstrate that increasing the magnetic field and dust particle density enhances fluid velocity while reducing temperature, leading to thinner momentum and thermal boundary layers. These effects are attributed to the Lorentz force, which accelerates fluid motion while reducing heat transfer efficiency. The findings provide valuable insights into MHD fluid flow applications, including pollutant dispersion and haze control on blunt surfaces. Additionally, this study is relevant to real-world applications such as cooling spherical electronic components, managing heat in nuclear fuel elements, and controlling thermal processes in plasma and metallurgical industries where dusty flows interact with magnetic fields. The novelty of this work lies in the simultaneous consideration of unsteady MHD effects, mixed convection, and dusty fluid interaction past a sphere, which has not been extensively addressed in previous studies. This integrated approach offers a more realistic framework for predicting heat transfer and flow behavior in complex engineering systems.

Keywords: dusty; magnetohydrodynamic; mixed convection; sphere.

1 Introduction

Two-phase or dusty Newtonian flow refers to the motion of rigid, spherical particles suspended in a Newtonian fluid. These particles are typically modeled as having uniform mass and size and are assumed to move nearly parallel to the carrier fluid with a small relative velocity, resulting in a low particle Reynolds number. Additionally, the particles are considered non-interacting and uniformly distributed throughout the fluid. The volume fraction of the dust phase is assumed to be negligible and is therefore excluded from the governing equations [9]. The presence of dust particles can significantly alter the flow momentum and heat transfer, which is crucial in various engineering, medical, and environmental applications [1]. Such flows play an important role in processes like nutrient transport [5], pollutant transport [3], groundwater treatment [24], polymer applications [2], and blood flow in arteries by modeling plasma as dust particles to study injured arteries [7].

When a magnetic field interacts with the fluid known as magnetohydrodynamics (MHD), it further modifies flow and thermal behavior, with practical relevance in environmental [13], solar aircraft wing [26] and in in medical applications (analyze blood flow [25], detect arterial injuries and diagnose abnormalities [20]). The presence of a magnetic field leads to a frictional force in the fluid flow [10]. Therefore, extensive research has addressed dusty fluid flow with MHD effects in boundary layer problems. Gao et al. [7] modeled blood flow as a dusty fluid to examine arterial behavior, while Henrique and Cunha [8] explored the effects of particle inertia on flow characteristics. Ali et al. [1] highlighted that the presence of MHD effects causes a reduction in fluid momentum due to the Lorentz force, which opposes fluid motion and has practical applications in gas-freezing systems and nuclear-powered reactors. Ru [23] found that MHD interactions within a suspension result in flow disruptions, leading to pressure variations in fluid particles. Furthermore, Sajjan et al. [24] concluded that as the magnetic field parameter rises, the fluid phase exhibits higher temperature and velocity compared to the dust phase, with the problem being numerically solved using MAPLE software. Chamkha and Ahmed [4] analyzed the influence of heat sources and chemical reactions at the front stagnation point of a sphere. Mohammad et al. [19] explored MHD effects on flow separation. Rajakumar et al. [21] and Mahdy and Nabwey [17] investigated related aspects such as slot suction, nanoparticles, and Newtonian heating. Raju et al. [22] studied the influence of an aligned magnetic field on drag.

In the past decades, there are some paper study on mixed convective flow past sphere without considering the influence of dust particles in the fluid flow. Khan et al. [15] and Mahdy et al. [18] investigated MHD effects on rotating spheres with mixed convection heat transfer. Dawar and Acharya [6] explored the effects of transient nanoparticles on thermal conductivity and profile, while Kumar et al. [16] applied the Keller-box method to investigate heat generation, thermal radiation, and absorption in the flow past a spinning sphere. This leaves a huge gap that can be seen. From the above mention, this reveals a significant research gap in examining MHD viscous fluid flow around a sphere with dusty mixed convective heat transfer. To fill this gap, the current study analyzes Newtonian fluid flow past a sphere, integrating MHD effects and dusty flow within a mixed convective heat transfer framework. Therefore, this study aims how dust particles influence velocity, temperature distribution, and boundary layer characteristics under varying magnetic field strengths and fluid-particle interactions. By employing numerical simulations via the Keller-box method, this research provides a deeper understanding of the interplay between dust particles, MHD force, and mixed convection heat transfer. The findings have potential applications in environmental and industrial systems, including haze control, pollutant dispersion, and cooling technologies.

Considering these practical implications, this study examines the influence of magnetohydrodynamics (MHD) on dusty mixed convective heat transfer around a spherical surface. Such a configuration is relevant to real-life applications, including electronic cooling, particulate-laden environmental flows, and magnetically controlled heat transfer in systems like plasma reactors and metallurgical processes. While many recent studies have focused on either MHD flow or dusty fluid dynamics, most have considered only simple geometries (such as flat plates or channels) and steady-state conditions. Furthermore, the combined effects of unsteady flow, MHD, mixed convection, and two-phase (dusty) interactions over a spherical geometry have not been comprehensively investigated. This work addresses that gap by developing a novel mathematical model that integrates all these factors in a unified formulation. By capturing these combined effects, the current study provides a more realistic and practical framework for analyzing heat and mass transfer in spherical geometries influenced by magnetic fields and particle suspensions, which are commonly encountered in both engineering and biomedical systems.

Nomenclature:

a	:	Radius of the sphere,
M	:	Magnetic parameter,
Pr	:	Prandtl number,
p	:	Non-dimensional pressure,
r	:	Non-dimensional radial axis of the sphere,
t	:	Non-dimensional time,
T	:	Non-dimensional temperature of fluid,
T_p	:	Non-dimensional temperature of dust particles,
u, v	:	Non-dimensional velocity components for $x-$ and $y-$axis,
$u_e(x)$	:	Non-dimensional external velocity,
x, y	:	Non-dimensional boundary layer coordinates measured along the surface of the sphere and normal to it, respectively,
μ	:	Dynamic viscosity,
σ	:	Electrical conductivity,
α	:	Mixed convection parameter,
ρ	:	Density of fluid,
ρ_p	:	Density of dust particles,
c_f	:	Specific heat of the fluid,
c_p	:	Specific heat of dust particles,
c	:	Fluid thermal conductivity,
τ_T	:	Thermal relaxation time of dust particles relative to the fluid,
τ_v	:	Relaxation time of dust particles relative to the fluid,
ν	:	Kinematic viscosity.

2 Problem Formulation

The fluid motion is characterized as a two-dimensional, dusty, viscous flow of an incompressible Newtonian fluid influenced by a magnetic field for an unsteady case. Initially at rest, the flow starts with velocity U_∞ at $\bar{t} = 0$, moving past an impulsively started sphere of radius a. This study is formulated using Cartesian coordinates $(\bar{x}, \bar{y})$ where $\bar{x}$ represents the dimensional $\bar{x}-$axis measured along the sphere's surface, starting from the forward stagnation point at $(\bar{x} = 0°)$ to the rear stagnation point at $(\bar{x} = 180°)$. The $\bar{y}-$axis corresponds to the normal direction to the sphere's surface. The sphere's temperature is assumed to be T_w, while the ambient fluid temperature is T_∞. The direction of the applied magnetic field, B_0, is considered to be perpendicular to the reference velocity, U_∞, while the direction of the gravitational force, $\bar{g}$, is opposite to the direction of the fluid flow. Figure 1 presents a graphical representation of the fluid flow model.

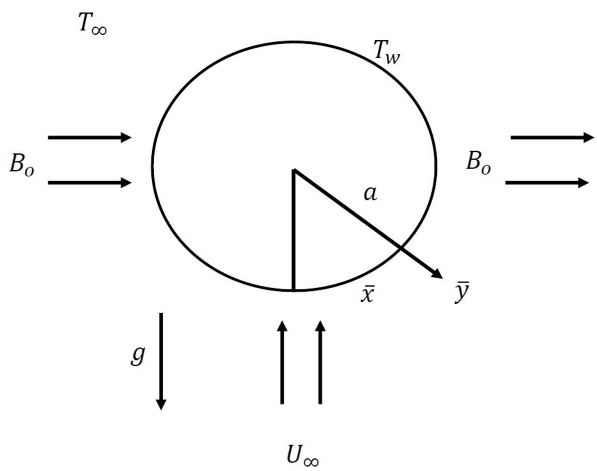

Figure 1: Physical coordinate of the problem.

The governing equations for unsteady mixed convective heat transfer past a sphere are adopted from Mohammad et al. [19], while the formulation for the dusty fluid flow is based on Izani and Ali [9]. The corresponding boundary conditions are defined in line with these references. The complete set of governing equations is presented below;

Fluid phase:
Continuity equation:

$$\frac{\partial(\bar{r}\bar{u})}{\partial\bar{x}} + \frac{\partial(\bar{r}\bar{v})}{\partial\bar{y}} = 0. \tag{1}$$

$\bar{x}-$momentum:

$$\frac{\partial\bar{u}}{\partial\bar{t}} + \bar{u}\frac{\partial\bar{u}}{\partial\bar{x}} + \bar{v}\frac{\partial\bar{u}}{\partial\bar{y}} = -\frac{1}{\rho}\frac{d\bar{p}}{d\bar{x}} + \frac{\mu}{\rho}\left(\frac{\partial^2\bar{u}}{\partial\bar{x}^2} + \frac{\partial^2\bar{u}}{\partial\bar{y}^2}\right) - \frac{\sigma B_o\bar{u}}{\rho} + \frac{\rho_p}{\rho}\left(\frac{\bar{u}_p - \bar{u}}{\tau_v}\right) + \alpha\bar{T}\sin(\bar{x}). \tag{2}$$

$\bar{y}-$momentum:

$$\frac{\partial\bar{v}}{\partial\bar{t}} + \bar{u}\frac{\partial\bar{v}}{\partial\bar{x}} + \bar{v}\frac{\partial\bar{v}}{\partial\bar{y}} = -\frac{1}{\rho}\frac{d\bar{p}}{d\bar{y}} + \frac{\mu}{\rho}\left(\frac{\partial^2\bar{v}}{\partial\bar{x}^2} + \frac{\partial^2\bar{v}}{\partial\bar{y}^2}\right) - \frac{\sigma B_o\bar{v}}{\rho} + \frac{\rho_p}{\rho}\left(\frac{\bar{v}_p - \bar{v}}{\tau_v}\right) + \alpha\bar{T}\cos(\bar{x}). \tag{3}$$

Energy equation:

$$\frac{\partial\bar{T}}{\partial\bar{t}} + \bar{u}\frac{\partial\bar{T}}{\partial\bar{x}} + \bar{v}\frac{\partial\bar{T}}{\partial\bar{y}} = \frac{c}{\rho c_f}\left(\frac{\partial^2\bar{u}}{\partial\bar{x}^2} + \frac{\partial^2\bar{u}}{\partial\bar{y}^2}\right) + \frac{\rho_p c_p}{\rho c_f}\left(\frac{\bar{T}_p - \bar{T}}{\tau_T}\right). \tag{4}$$

Dust phase:
Continuity equation:

$$\frac{\partial(\bar{r}\bar{u_p})}{\partial\bar{x}} + \frac{\partial(\bar{r}\bar{v_p})}{\partial\bar{y}} = 0. \tag{5}$$

$\bar{x}-$momentum:

$$\frac{\partial \bar{u}_p}{\partial \bar{t}} + \bar{u}_p \frac{\partial \bar{u}_p}{\partial \bar{x}} + \bar{v}_p \frac{\partial \bar{u}_p}{\partial \bar{y}} = \frac{\bar{u} - \bar{u}_p}{\tau_v}. \tag{6}$$

$\bar{y}-$momentum:

$$\frac{\partial \bar{v}_p}{\partial \bar{t}} + \bar{u}_p \frac{\partial \bar{v}_p}{\partial \bar{x}} + \bar{v}_p \frac{\partial \bar{v}_p}{\partial \bar{y}} = \frac{\bar{v} - \bar{v}_p}{\tau_v}. \tag{7}$$

Energy equation:

$$\frac{\partial \bar{T}_p}{\partial \bar{t}} + \bar{u}_p \frac{\partial \bar{T}_p}{\partial \bar{x}} + \bar{v}_p \frac{\partial \bar{T}_p}{\partial \bar{y}} = \frac{\bar{T} - \bar{T}_p}{\tau_T}. \tag{8}$$

with the initial and boundary conditions;

$$\begin{aligned}
&\bar{t} < 0 : \bar{u} = \bar{v} = \bar{u}_p = \bar{v}_p = 0, \qquad \bar{T} = T_\infty, \forall \bar{x}\ , \bar{y}, \\
&\bar{t} \geq 0 : \bar{u} = \bar{v} = 0, \qquad \bar{T} = T_w, \qquad \bar{y} = 0, \\
&\bar{t} \geq 0 : \bar{u}_e(\bar{x}) = U_w, \qquad \bar{u}_p \to 1, \qquad \bar{v}_p \to \bar{v}, \qquad \bar{T} = T_\infty, \qquad \bar{T}_p = T_\infty, \qquad \bar{y} \to \infty,
\end{aligned} \tag{9}$$

where $\bar{r}$ is the distance from the symmetrical axis to the sphere's surface in the radial direction,$\bar{u}$, $\bar{v}$ and $\bar{u}_p$, $\bar{v}_p$ are the velocity components of the fluid and dust particles, $\bar{p}$ is the pressure, $\bar{T}$ is the dimensional temperature of the fluid, $\bar{t}$ is the dimensional time and $\bar{u}_e$ is the stream velocity. Subsequently, the governing equations are represented using the corresponding nondimensional variables [12],

$$\begin{aligned}
&t = U_\infty \frac{\bar{t}}{a}, \quad x = \frac{\bar{x}}{a}, \quad y = \mathrm{Re}^{1/2} \frac{\bar{y}}{a}, \quad u = \frac{\bar{u}}{U_\infty}, \quad v = \mathrm{Re}^{1/2} \frac{\bar{v}}{U_\infty}, \quad u_p = \frac{\bar{u}_p}{U_\infty}, \\
&v_p = \mathrm{Re}^{1/2} \frac{\bar{v}_p}{U_\infty}, \quad p = \frac{\bar{p}}{\rho U_\infty^2}, \quad r = \frac{\bar{r}(\bar{x})}{a}, \quad T = \frac{\bar{T} - T_\infty}{\bar{T}_w - T_\infty}, \quad T_p = \frac{\bar{T}_p - T_\infty}{\bar{T}_w - T_\infty},
\end{aligned} \tag{10}$$

with non-imensional numbers as below:

$Re = \dfrac{\rho a U_\infty}{\mu}$ is the Reynolds number, $\nu = \dfrac{\mu}{\rho}$ is the kinematic viscosity,

$M = \dfrac{a \sigma B_0^2}{\rho U_\infty}$ is the magnetic parameter, $Pr = \dfrac{\nu \rho c_f}{c}$ is the Prandtl number,

$\beta_T = \dfrac{a}{U_\infty \tau_T}$ is the local fluid particle for temperature, $\gamma = \dfrac{c_p}{c_f}$ is the specific heat ratio,

$\beta_v = \dfrac{a}{U_\infty \tau_v}$ is the local fluid particle interaction for velocity,

$G = \dfrac{\rho_p}{\rho}$ is the dust particles mass concentration parameter.

Outside the boundary layer region, the stream velocity, $\dfrac{\bar{u}_e^2}{2} + \bar{p} =$ constant, and the pressure will be $\dfrac{d\bar{p}}{d\bar{x}} = -\bar{u}_e \dfrac{d\bar{u}_e}{d\bar{x}}$, where $\bar{u}_e = \dfrac{3}{2}\sin(\bar{x})$ [11]. Thus, $-\dfrac{d\bar{p}}{d\bar{x}} = \bar{u}_e \dfrac{d\bar{u}_e}{d\bar{x}} + M\bar{u}_e$ and (1)−(9) become

Fluid phase:
Continuity equation:

$$\frac{\partial (ru)}{\partial x} + \frac{\partial (rv)}{\partial y} = 0. \tag{11}$$

$\bar{x}-$momentum:

$$\frac{\partial u}{\partial t} + u\frac{\partial u}{\partial x} + v\frac{\partial u}{\partial y} = u_e\frac{du_e}{dx} + \frac{\mu}{\rho}\left(\frac{\partial^2 u}{\partial x^2} + \frac{\partial^2 u}{\partial y^2}\right)\frac{\partial^2 u}{\partial y^2}\partial y + M\left(u_e - u\right) + \beta_v G\left(u_p - u\right) + \frac{2}{3}\alpha T. \tag{12}$$

Energy equation:

$$\frac{\partial T}{\partial t} + u\frac{\partial T}{\partial x} + v\frac{\partial T}{\partial y} = \frac{1}{\mathrm{Pr}}\frac{\partial^2 T}{\partial y^2} + \beta_T\gamma G\left(T_p - T\right). \tag{13}$$

Dust phase:
Continuity equation:

$$\frac{\partial (ru_p)}{\partial x} + \frac{\partial (rv_p)}{\partial y} = 0. \tag{14}$$

$\bar{x}-$momentum:

$$\frac{\partial u_p}{\partial t} + u_p\frac{\partial u_p}{\partial x} + v_p\frac{\partial u_p}{\partial y} = \beta_v\left(u - u_p\right). \tag{15}$$

Energy equation:

$$\frac{\partial T_p}{\partial t} + u_p\frac{\partial T_p}{\partial x} + v_p\frac{\partial T_p}{\partial y} = \beta_T\left(T - T_p\right), \tag{16}$$

associated to

$$\begin{aligned}
&t < 0 : u = v = u_p = v_p = 0, \quad T = T_\infty, \quad \forall\, x, y,\\
&t \geq 0 : u = v = 0, \quad T = 1, \quad y = 0,\\
&t \geq 0 : u_e(x) = u, \quad u_p \to 1, \quad v_p \to v, \quad T = 0, \quad T_p = 0, \quad y \to \infty.
\end{aligned} \tag{17}$$

To simplify and optimize the mathematical model, the stream function is utilized to reduce the complexity of the governing equations. In this study, the small-time ($t < t^*$) and large-time ($t > t^*$) cases are utilized to eliminate singularities at specific time points [19],

$$u = \frac{1}{r}\frac{\partial \psi}{\partial y}, v = -\frac{1}{r}\frac{\partial \psi}{\partial x}, u_p = \frac{1}{r}\frac{\partial \psi_p}{\partial y}, v_p = -\frac{1}{r}\frac{\partial \psi_p}{\partial x}, \tag{18}$$

where

For small time:

$$\begin{aligned}
\eta &= \frac{y}{t^{1/2}},\\
\psi &= t^{1/2}u_e(x)r(x)f(x,\eta,t),\\
\psi_p &= t^{1/2}u_e(x)r(x)h(x,\eta,t),\\
T &= s(x,\eta,t),\\
T_p &= g(x,\eta,t).
\end{aligned} \tag{19}$$

For large time:

$$\begin{aligned} \eta &= y, \\ \psi &= u_e(x)r(x)f(x,\eta,t), \\ \psi_p &= u_e(x)r(x)h(x,\eta,t), \\ T &= s(x,\eta,t), \\ T_p &= g(x,\eta,t). \end{aligned} \tag{20}$$

The forward stagnation point is applied in this study as $u_e(x) = 0$ when $x = 0^{\circ}$ with implies $\dfrac{du_e}{dx} = \dfrac{3}{2}$. The equations for the small-time case is as here,

$$f''' + \frac{\eta}{2}f'' + \frac{3}{2}t(1-(f')^2 + ff'') + Mt(1-f') + \beta_v Gt(h'-f') = t\frac{\partial f'}{\partial t}, \tag{21}$$

$$s'' + \mathrm{Pr}\frac{\eta}{2}s' + \mathrm{Pr}t\frac{3}{2}tfs' + \mathrm{Pr}\beta_T\gamma Gt(g-s) = \mathrm{Pr}t\frac{\partial s}{\partial t}, \tag{22}$$

$$\frac{\eta}{2}h'' + \frac{3}{2}t(hh''-(h')^2) + \beta_v t(f'-h') = t\frac{\partial h'}{\partial t}, \tag{23}$$

$$\frac{\eta}{2}g' + \frac{3}{2}thg' + \beta_T t(s-g) = t\frac{\partial g}{\partial t}, \tag{24}$$

and (17) becomes,

$$\begin{aligned} &t<0: f=f'=h=h'=0, \quad s=0, \quad \forall\, x,\eta, \\ &t\geq 0: f=f'=0, \quad s=1, \quad \eta=0, \\ &t\geq 0: f'=1, \quad h'\to 1, \quad h\to f, \quad s=0, \quad g=0, \quad \eta\to\infty. \end{aligned} \tag{25}$$

For large time case:

$$f''' + \frac{3}{2}(1-(f')^2 + ff'') + M(1-f') + \beta_v G(h'-f') + \frac{2}{3}\alpha s = \frac{\partial f'}{\partial t}, \tag{26}$$

$$s'' + \mathrm{Pr}\frac{3}{2}fs' + \mathrm{Pr}\beta_T\gamma G(g-s) = \mathrm{Pr}\frac{\partial s}{\partial t}, \tag{27}$$

$$\frac{3}{2}(hh''-(h')^2) + \beta_v(f'-h') = \frac{\partial h'}{\partial t}, \tag{28}$$

$$\frac{3}{2}hg' + \beta_T(s-g) = \frac{\partial g}{\partial t}, \tag{29}$$

subject to

$$\begin{aligned} &f=f'=0, \quad s=1, \quad \eta=0, \\ &f'=1, \quad h'\to 1, \quad h\to f, \quad s=0, \quad g=0, \quad \eta\to\infty. \end{aligned} \tag{30}$$

Kasim et al. [14] indicated that exact solutions can be determined by solving the governing equation directly. Therefore, the exact solution can be derived from (21) and (22) concerning the initial and boundary conditions (25). Thus, the validating benchmark of this study will be,

$$f = \eta \text{erf}\left(\frac{\eta}{2}\right) + \frac{2}{\sqrt{\pi}} \exp\left(\frac{\eta^2}{4} - 1\right), \tag{31}$$

$$f' = \text{erf}\left(\frac{\eta}{2}\right), \tag{32}$$

$$f'' = \frac{1}{\sqrt{\pi}} \exp\left[\frac{-\eta^2}{4}\right], \tag{33}$$

$$s = 1 - \text{erf}\left(\frac{\sqrt{\text{Pr}}}{2}\eta\right), \tag{34}$$

$$s' = -\sqrt{\frac{\text{Pr}}{\pi}} \exp\left(-\frac{\text{Pr}}{4}\eta^2\right). \tag{35}$$

3 Numerical Solution

By applying a similarity transformation, the higher-order partial differential equations (PDEs) for both small and large cases are simplified into first-order PDEs. The Keller-box approach is then applied using linearization through the finite difference method, Newton's method, and the construction of a block tri-diagonal structure. MATLAB software is then utilized to solve the Keller-box method and visually interpret the parameters. The Keller box is shown here. For small time case, new variables for the implementations of these numerical techniques as below,

$$f' = u, \qquad u' = v, \qquad s' = q, \qquad h' = p. \tag{36}$$

Equations (21)−(24) transformed as below,

$$v' + \frac{\eta}{2}v + \frac{3}{2}t(1 - u^2 + fv) + Mt(1 - u) + \beta_v Gt(p - u) + \frac{2}{3}\alpha ts = t\frac{\partial u}{\partial t}, \tag{37}$$

$$q' + \text{Pr}\frac{\eta}{2}q + \text{Pr}\frac{3}{2}tfq + \text{Pr}\beta_T\gamma Gt(g - s) = \text{Pr}t\frac{\partial s}{\partial t}, \tag{38}$$

$$\frac{\eta}{2}p' + \frac{3}{2}t(hp' - p^2) + \beta_v t(u - p) = t\frac{\partial p}{\partial t}, \tag{39}$$

$$\frac{\eta}{2}g' + \frac{3}{2}thg' + \beta_T t(s - g) = t\frac{\partial g}{\partial t}, \tag{40}$$

with

$$\begin{aligned}
&t < 0 : f = u = h = p = 0, \qquad s = 0, \forall x, \eta, \\
&t \geq 0 : f = u = 0, \qquad s = 1, \qquad \eta = 0, \\
&t \geq 0 : u = 1, \qquad p \to 1, \qquad h \to f, \qquad s = 0, \qquad g = 0, \qquad \eta \to \infty.
\end{aligned} \tag{41}$$

By using finite differences, (36)−(40) reduces to

$$\frac{f_j^n - f_{j-1}^n}{l_j} - u_{j-1/2}^n = 0, \tag{42}$$

$$\frac{u_j^n - u_{j-1}^n}{l_j} - v_{j-1/2}^n = 0, \tag{43}$$

$$\frac{s_j^n - s_{j-1}^n}{l_j} - q_{j-1/2}^n = 0, \tag{44}$$

$$\frac{h_j^n - h_{j-1}^n}{l_j} - p_{j-1/2}^n = 0, \tag{45}$$

$$\begin{aligned}
&\frac{1}{l_j}\left(v_j^n - v_{j-1}^n\right) + \frac{\eta_{j-1/2}^n}{2} v_{j-1/2}^n + \frac{3}{2} t^{n-1/2}\Big[1 - (u_{j-1/2}^n)^2 + (fv)_{j-1/2}^n)^2\Big] + M t^{n-1/2}(1 - u_{j-1/2}^n) \\
&+ \beta_v G t^{n-1/2}(p_{j-1/2}^n - u_{j-1/2}^n) + \frac{2}{3}\alpha t^{n-1/2} s_{j-1/2}^n - 2t^{n-1/2}\frac{u_{j-1/2}^n}{k_n} \\
&\quad = -\frac{1}{l_j}(v_{j-1}^{n-1} - v_{j-1/2}^{n-1}) - \frac{\eta_{j-1/2}^n}{2} v_{j-1/2}^{n-1} - \frac{3}{2} t^{n-1/2}\Big[1 - (u^2)_{j-1/2}^{n-1} + (fv)_{j-1/2}^{n-1})\Big] \\
&\qquad - M t^{n-1/2}(1 - u_{j-1/2}^{n-1}) - \beta_v G t^{n-1/2}(p_{j-1/2}^{n-1} - u_{j-1/2}^{n-1}) - \frac{2}{3}\alpha t^{n-1/2} s_{j-1/2}^{n-1} \\
&\qquad - 2t^{n-1/2}\frac{u_{j-1/2}^{n-1}}{k_n},
\end{aligned} \tag{46}$$

$$\begin{aligned}
&\frac{1}{l_j}(q_j^n - q_{j-1}^n) + \Pr\frac{\eta_{j-1/2}}{2} q_{j-1/2}^n + \frac{3}{2}\Pr t^{n-1/2}(fq)_{j-1/2}^n + \Pr\beta_T\gamma G t^{n-1/2}(g_{j-1/2}^n - s_{j-1/2}^n) \\
&- 2Pr\, t^{n-1/2}\frac{s_{j-1/2}^n}{k_n} = -\frac{1}{l_j}(q_j^{n-1} - q_{j-1}^{n-1}) - \Pr\frac{\eta_{j-1/2}}{2} q_{j-1/2}^{n-1} - \frac{3}{2}\Pr t^{n-1/2}(fq)_{j-1/2}^{n-1} \\
&\qquad - \Pr\beta_T\gamma G t^{n-1/2}(g_{j-1/2}^{n-1} - s_{j-1/2}^{n-1}) - 2Pr\, t^{n-1/2}\frac{s_{j-1/2}^{n-1}}{k_n},
\end{aligned} \tag{47}$$

$$\begin{aligned}
&\frac{\eta_{j-1/2}}{2}(p_j^n - p_{j-1}^n) + \frac{3}{2} t^{n-1/2}(h_{j-1/2}^n\big[p_j^n - p_{j-1}^n\big] - (p^2)_{j-1/2}^n) + \beta_v t^{n-1/2}(u_{j-1/2}^n - p_{j-1/2}^n) \\
&- 2t^{n-1/2}\frac{p_{j-1/2}^n}{k_n} = -\frac{\eta_{j-1/2}}{2}(p_j^{n-1} - p_{j-1}^{n-1}) - \frac{3}{2} t^{n-1/2}(h_{j-1/2}^{n-1}\big[p_j^{n-1} - p_{j-1}^{n-1}\big] \\
&\qquad - (p^2)_{j-1/2}^{n-1}) - \beta_v t^{n-1/2}(u_{j-1/2}^{n-1} - p_{j-1/2}^{n-1}) - 2t^{n-1/2}\frac{p_{j-1/2}^{n-1}}{k_n},
\end{aligned} \tag{48}$$

$$\begin{aligned}
&\frac{\eta_{j-1/2}}{2}(g_j^n - g_{j-1}^n) + \frac{3}{2} t^{n-1/2} h_{j-1/2}^n\big[g_j^n - g_{j-1}^n\big] + t^{n-1/2}\beta_T(s_{j-1/2}^n - g_{j-1/2}^n) - 2t^{n-1/2}\frac{g_{j-1/2}^n}{k_n} \\
&\quad = -\frac{\eta_{j-1/2}}{2}(g_j^{n-1} - g_{j-1}^{n-1}) - \frac{3}{2} t^{n-1/2} h_{j-1/2}^{n-1}\big[g_j^{n-1} - g_{j-1}^{n-1}\big] - t^{n-1/2}\beta_T(s_{j-1/2}^{n-1} - g_{j-1/2}^{n-1}) \\
&\qquad - 2t^{n-1/2}\frac{g_{j-1/2}^{n-1}}{k_n}.
\end{aligned} \tag{49}$$

Here, $j = 1, 2, \ldots, J$ and $n = 1, 2, \ldots, N$ denote the spatial grid index and time level index, respectively, where J is the total number of spatial grid intervals and N is the total number of time steps. The terms l_j and k_n in the above equations represent the grid spacing and the time increment, respectively.

Then, Newton's method is applied as shown,

$$\delta f_j - \delta f_{j-1} - \frac{l_j}{2}(\delta u_j - \delta u_{j-1}) = (r_1)_j, \tag{50}$$

$$\delta u_j - \delta u_{j-1} - \frac{l_j}{2}(\delta u_j - \delta u_{j-1}) = (r_2)_j, \tag{51}$$

$$\delta f_j - \delta f_{j-1} - \frac{l_j}{2}(\delta u_j - \delta u_{j-1}) = (r_3)_j, \tag{52}$$

$$\delta f_j - \delta f_{j-1} - \frac{l_j}{2}(\delta u_j - \delta u_{j-1}) = (r_4)_j, \tag{53}$$

$$\begin{aligned}(s_1)\delta v_j + (s_2)\delta v_{j-1} + (s_3)\delta u_j + (s_4)\delta u_{j-1} + (s_5)\delta f_j + (s_6)\delta f_{j-1} \\ +(s_7)\delta p_j + (s_8)\delta p_{j-1} + (s_9)\delta s_j + (s_{10})\delta s_{j-1} = (r_5)_j,\end{aligned} \tag{54}$$

$$\begin{aligned}(b_1)\delta q_j + (b_2)\delta q_{j-1} + (b_3)\delta s_j + (b_4)\delta s_{j-1} + (b_5)\delta f_j + (b_6)\delta f_{j-1} \\ +(b_7)\delta g_j + (b_8)\delta g_{j-1} = (r_6)_j,\end{aligned} \tag{55}$$

$$(c_1)\delta p_j + (c_2)\delta p_{j-1} + (c_3)\delta h_j + (c_4)\delta h_{j-1} + (c_5)\delta u_j + (c_6)\delta u_{j-1} = (r_7)_j, \tag{56}$$

$$(d_1)\delta g_j + (d_2)\delta g_{j-1} + (d_3)\delta h_j + (d_4)\delta h_{j-1} + (d_5)\delta s_j + (d_6)\delta s_{j-1} = (r_8)_j, \tag{57}$$

where

$$\begin{aligned}
(s_1)_j &= \frac{1}{l_j} + \frac{\eta_{j-1/2}}{4} + \frac{3}{4}t^{n-1/2}f_j^n,\\
(s_2)_j &= -\frac{1}{l_j} + \frac{\eta_{j-1/2}}{4} + \frac{3}{4}t^{n-1/2}f_{j-1}^n,\\
(s_3)_j &= -\frac{3}{4}t^{n-1/2}u_j^n - M\frac{t^{n-1/2}}{2} - \beta_v G\frac{t_{n-1/2}}{2} - \frac{t_{n-1/2}}{k_n},\\
(s_4)_j &= -\frac{3}{4}t^{n-1/2}u_{j-1}^n - M\frac{t^{n-1/2}}{2} - \beta_v G\frac{t_{n-1/2}}{2} - \frac{t_{n-1/2}}{k_n},\\
(s_5)_j &= \frac{3}{4}t^{n-1/2}v_j^n,\\
(s_6)_j &= \frac{3}{4}t^{n-1/2}v_{j-1}^n,\\
(s_7)_j &= \beta_v G\frac{t_{n-1/2}}{2} = (s_8)_j,\\
(s_9)_j &= \alpha\frac{t_{n-1/2}}{3} = (s_{10})_j,
\end{aligned} \tag{58}$$

$$
\begin{aligned}
(b_1)_j &= \frac{1}{l_j} + \mathrm{Pr}\frac{\eta_{j-1/2}}{4} + \mathrm{Pr}\frac{3}{4}t^{n-1/2}f_j^n,\\
(b_2)_j &= -\frac{1}{l_j} + \mathrm{Pr}\frac{\eta_{j-1/2}}{4} + \mathrm{Pr}\frac{3}{4}t^{n-1/2}f_{j-1}^n,\\
(b_3)_j &= \mathrm{Pr}\frac{3}{4}t^{n-1/2}q_j^n,\\
(b_4)_j &= \mathrm{Pr}\frac{3}{4}t^{n-1/2}q_{j-1}^n,\\
(b_5)_j &= \mathrm{Pr}\frac{\beta_T G\gamma}{2}t^{n-1/2} = (b_6)_j,\\
(b_7)_j &= -\mathrm{Pr}\frac{\beta_T G\gamma}{2}t^{n-1/2} - \mathrm{Pr}\frac{t_{n-1/2}}{k_n} = (b_8)_j,
\end{aligned}
\tag{59}
$$

$$
\begin{aligned}
(c_1)_j &= \frac{\eta}{2l_j} + \frac{3}{2l_j}t^{n-1/2}h_j^n - \frac{3}{2}t^{n-1/2}p_j^n - \beta_v\frac{t^{n-1/2}}{2} - \frac{t^{n-1/2}}{k_n},\\
(c_2)_j &= -\frac{\eta}{2l_j} + \frac{3}{2l_j}t^{n-1/2}h_{j-1}^n - \frac{3}{2}t^{n-1/2}p_{j-1}^n - \beta_v\frac{t^{n-1/2}}{2} - \frac{t^{n-1/2}}{k_n},\\
(c_3)_j &= \frac{3}{2l_j}t^{n-1/2}p_j^n,\\
(c_4)_j &= \frac{3}{2l_j}t^{n-1/2}p_{j-1}^n,\\
(c_5)_j &= \beta_v\frac{t^{n-1/2}}{2} = (c_6)_j,
\end{aligned}
\tag{60}
$$

$$
\begin{aligned}
(d_1)_j &= \frac{\eta}{2l_j} + \frac{3}{2l_j}t^{n-1/2}h_j^n - \beta_v\frac{t^{n-1/2}}{2} - \frac{t^{n-1/2}}{k_n},\\
(d_2)_j &= -\frac{\eta}{2l_j} + \frac{3}{2l_j}t^{n-1/2}h_{j-1}^n - \beta_v\frac{t^{n-1/2}}{2} - \frac{t^{n-1/2}}{k_n},\\
(d_3)_j &= \frac{3}{2l_j}t^{n-1/2}g_j^n,\\
(d_4)_j &= \frac{3}{2l_j}t^{n-1/2}g_{j-1}^n,\\
(d_5)_j &= \beta_T\frac{t^{n-1/2}}{2} = (d_6)_j,
\end{aligned}
\tag{61}
$$

$$
\begin{aligned}
(r_1)_j &= f_{j-1}^n - f_j^n + l_j u_{j-1/2}^n,\\
(r_2)_j &= u_{j-1}^n - u_j^n + l_j v_{j-1/2}^n,\\
(r_3)_j &= s_{j-1}^n - s_j^n + l_j q_{j-1/2}^n,\\
(r_4)_j &= h_{j-1}^n - h_j^n + l_j p_{j-1/2}^n,
\end{aligned}
\tag{62}
$$

$$
\begin{aligned}
(r_5)_j = &-\frac{1}{l_j}\left(v_j^n - v_{j-1}^n\right) - \frac{\eta_{j-1/2}^n}{2}v_{j-1/2}^n - \frac{3}{2}t^{n-1/2}\Big[1 - (u_{j-1/2}^n)^2 + (fv)_{j-1/2}^n)^2\Big] \\
&- Mt^{n-1/2}(1 - u_{j-1/2}^n) - \beta_v G t^{n-1/2}(p_{j-1/2}^n - u_{j-1/2}^n) - \frac{2}{3}\alpha t^{n-1/2}s_{j-1/2}^n \\
&+ 2t^{n-1/2}\frac{u_{j-1/2}^n}{k_n} - \frac{1}{l_j}(v_{j-1}^{n-1} - v_{j-1/2}^{n-1}) - \frac{\eta_{j-1/2}^n}{2}v_{j-1/2}^{n-1} \\
&- \frac{3}{2}t^{n-1/2}\Big[1 - (u^2)_{j-1/2}^{n-1} + (fv)_{j-1/2}^{n-1})\Big] - Mt^{n-1/2}(1 - u_{j-1/2}^{n-1}) \\
&- \beta_v G t^{n-1/2}(p_{j-1/2}^{n-1} - u_{j-1/2}^{n-1}) - \frac{2}{3}\alpha t^{n-1/2}s_{j-1/2}^{n-1} - 2t^{n-1/2}\frac{u_{j-1/2}^{n-1}}{k_n},
\end{aligned} \tag{63}
$$

$$
\begin{aligned}
(r_6)_j = &-\frac{1}{l_j}(q_j^n - q_{j-1}^n) - \Pr\frac{\eta_{j-1/2}}{2}q_{j-1/2}^n - \frac{3}{2}\Pr t^{n-1/2}(fq)_{j-1/2}^n \\
&- \Pr\beta_T\gamma G t^{n-1/2}(g_{j-1/2}^n - s_{j-1/2}^n) + 2Pr\, t^{n-1/2}\frac{s_{j-1/2}^n}{k_n} - \frac{1}{l_j}(q_j^{n-1} - q_{j-1}^{n-1}) \\
&- \Pr\frac{\eta_{j-1/2}}{2}q_{j-1/2}^{n-1} - \frac{3}{2}\Pr t^{n-1/2}(fq)_{j-1/2}^{n-1} - \Pr\beta_T\gamma G t^{n-1/2}(g_{j-1/2}^{n-1} - s_{j-1/2}^{n-1}) \\
&- 2\Pr t^{n-1/2}\frac{s_{j-1/2}^{n-1}}{k_n},
\end{aligned} \tag{64}
$$

$$
\begin{aligned}
(r_7)_j = &-\frac{\eta_{j-1/2}}{2}(p_j^n - p_{j-1}^n) - \frac{3}{2}t^{n-1/2}(h_{j-1/2}^n\big[p_j^n - p_{j-1}^n\big] - (p^2)_{j-1/2}^n) \\
&- \beta_v t^{n-1/2}(u_{j-1/2}^n - p_{j-1/2}^n) + 2t^{n-1/2}\frac{p_{j-1/2}^n}{k_n} - \frac{\eta_{j-1/2}}{2}(p_j^{n-1} - p_{j-1}^{n-1}) \\
&- \frac{3}{2}t^{n-1/2}(h_{j-1/2}^{n-1}\big[p_j^{n-1} - p_{j-1}^{n-1}\big] - (p^2)_{j-1/2}^{n-1}) - \beta_v t^{n-1/2}(u_{j-1/2}^{n-1} - p_{j-1/2}^{n-1}) \\
&- 2t^{n-1/2}\frac{p_{j-1/2}^{n-1}}{k_n},
\end{aligned} \tag{65}
$$

$$
\begin{aligned}
(r_8)_j = &-\frac{\eta_{j-1/2}}{2}(g_j^n - g_{j-1}^n) - \frac{3}{2}t^{n-1/2}h_{j-1/2}^n\big[g_j^n - g_{j-1}^n\big] - t^{n-1/2}\beta_T(s_{j-1/2}^n - g_{j-1/2}^n) \\
&+ 2t^{n-1/2}\frac{g_{j-1/2}^n}{k_n} - \frac{\eta_{j-1/2}}{2}(g_j^{n-1} - g_{j-1}^{n-1}) - \frac{3}{2}t^{n-1/2}h_{j-1/2}^{n-1}\big[g_j^{n-1} - g_{j-1}^{n-1}\big] \\
&- t^{n-1/2}\beta_T(s_{j-1/2}^{n-1} - g_{j-1/2}^{n-1}) - 2t^{n-1/2}\frac{g_{j-1/2}^{n-1}}{k_n}.
\end{aligned} \tag{66}
$$

The matrix form of a given system of the equation is reduced into a tri-diagonal form and then solved by using LU factorization,

$$
\begin{aligned}
[A_1][\delta_1] + [C_1][\delta_2] &= [r_1],\\
[B_1][\delta_1] + [A_2][\delta_2] + [C_1][\delta_3] &= [r_2],\\
-------------&\\
[B_{j-1}][\delta_1] + [A_{j-1}][\delta_2] + [C_{j-1}][\delta_3] &= [r_{j-1}],\\
[B_j][\delta_{j-1}] + [A_j][\delta_j] &= [r_j], \qquad \text{for } j = 1, 2, 3, \ldots,
\end{aligned}
\tag{67}
$$

where

$$
A_1 = \begin{bmatrix}
0 & 0 & 0 & 0 & 0 & 1 & 0 & 0\\
-0.5l_j & 0 & 0 & 0 & 0 & 0 & -0.5l_j & 0\\
0 & -0.5l_j & 0 & 0 & 0 & 0 & 0 & -0.5l_j\\
0 & 0 & -1 & -0.5l_j & 0 & 0 & 0 & 0\\
(s_2)_j & 0 & 0 & (s_8)_j & 0 & (s_5)_j & (s_1)_j & 0\\
0 & (b_2)_j & 0 & 0 & (b_6)_j & (b_3)_j & 0 & (b_1)_j\\
0 & 0 & (c_4)_j & (c_2)_j & 0 & 0 & 0 & 0\\
0 & 0 & (d_4)_j & 0 & (d_2)_j & 0 & 0 & 0
\end{bmatrix},
$$

$$
A_j = \begin{bmatrix}
-0.5l_j & 0 & 0 & 0 & 0 & 1 & 0 & 0\\
-1 & 0 & 0 & 0 & 0 & 0 & -0.5l_j & 0\\
0 & 0 & 0 & -1 & 0 & 0 & 0 & -0.5l_j\\
0 & -0.5l_j & -1 & 0 & 0 & 0 & 0 & 0\\
(s_4)_j & (s_8)_j & 0 & 0 & 0 & (s_5)_j & (s_1)_j & 0\\
0 & 0 & 0 & (b_8)_j & (b_6)_j & (b_3)_j & 0 & (b_1)_j\\
(c_6)_j & (c_2)_j & (c_4)_j & 0 & 0 & 0 & 0 & 0\\
0 & 0 & (d_4)_j & (d_6)_j & (d_2)_j & 0 & 0 & 0
\end{bmatrix}, \qquad 2 \le j \le J,
$$

$$
B_j = \begin{bmatrix}
0 & 0 & 0 & 0 & 0 & -1 & 0 & 0\\
0 & 0 & 0 & 0 & 0 & 0 & -0.5l_j & 0\\
0 & 0 & 0 & 0 & 0 & 0 & 0 & -0.5l_j\\
0 & 0 & 0 & 0 & 0 & 0 & 0 & 0\\
0 & 0 & 0 & 0 & 0 & (s_6)_j & (s_2)_j & 0\\
0 & 0 & 0 & 0 & 0 & (b_4)_j & 0 & (b_2)_j\\
0 & 0 & 0 & 0 & 0 & 0 & 0 & 0\\
0 & 0 & 0 & 0 & 0 & 0 & 0 & 0
\end{bmatrix}, \qquad 1 \le j \le J-1,
$$

$$
C_j = \begin{bmatrix}
-0.5l_j & 0 & 0 & 0 & 0 & 0 & 0 & 0\\
1 & 0 & 0 & 0 & 0 & 0 & 0 & 0\\
0 & 0 & 0 & 1 & 0 & 0 & 0 & 0\\
0 & -0.5l_j & 1 & 0 & 0 & 0 & 0 & 0\\
(s_3)_j & (s_7)_j & 0 & 0 & 0 & 0 & 0 & 0\\
0 & 0 & 0 & (b_7)_j & (b_5)_j & 0 & 0 & 0\\
(c_5)_j & (c_1)_j & (c_3)_j & 0 & 0 & 0 & 0 & 0\\
0 & 0 & (d_3)_j & (d_5)_j & (d_1)_j & 0 & 0 & 0
\end{bmatrix}, \qquad 2 \le j \le J.
$$

In this study, the values of $\triangle\eta$ and $\triangle t$ are set to 0.01 and 0.05, respectively. For the numerical solution, the initial guess is obtained by solving (21) and (22) at time $t = 0$. At this initial time, the velocity of the dust phase is assumed to be equal to the momentum and energy values of the fluid. A convergence criterion of 10^{-6} is employed in the numerical calculations to obtain stable and accurate solutions. This assumption ensures a consistent and physically reasonable starting profile for the Keller box method, facilitating stable and accurate convergence. The accuracy of the results was validated by comparing them with the exact solutions from (33) and (35). The numerical comparison between the numerical and exact solutions for $f''(\eta)$ and $-s(\eta)$ is presented in Table 1, and graphically plotted in Figures 2 and 3.

Table 1: Validation of $f''(\eta)$ and $-s'(\eta)$ as $\beta_v = \beta_T = \gamma = G = 0$ at $t = 0$ and Pr$= 0.7$.

η	$f''(\eta)$			$-s'(\eta)$		
	Exact equation (33)	Present (numerical solution)	Residual squared error	Exact equation (35)	Present (numerical solution)	Residual squared error
0.0	0.5642	0.5642	0.0000	-0.4720	-0.4720	0.0000
0.5	0.5300	0.5300	0.0000	-0.4518	-0.4518	0.0000
1.0	0.4394	0.4394	0.0000	-0.3963	-0.3963	0.0000
1.5	0.3215	0.3215	0.0000	-0.3184	-0.3184	0.0000
2.0	0.2076	0.2076	0.0000	-0.2344	-0.2344	0.0000

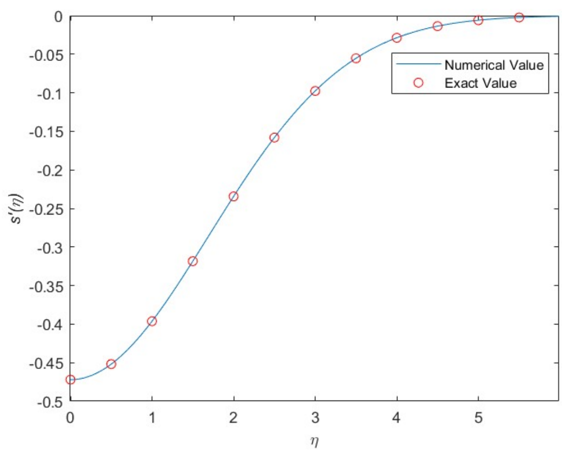

Figure 2: Comparison of $f''(\eta)$ between numerical and exact value.

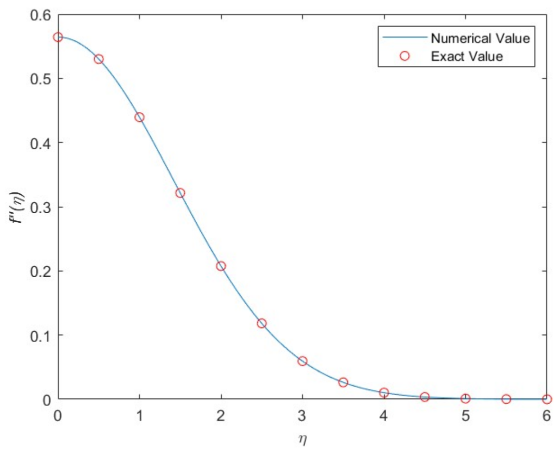

Figure 3: Comparison of $-s'(\eta)$ between numerical and exact value.

4 Results and Discussion

This section analyzes the findings for the forward stagnation point, highlighting velocity and temperature profiles at $t = 1.5$ for different values of M, G, β_v, β_T and γ, with $\Pr = 0.7$. The velocity of fluid $f'(\eta)$, the velocity of dust particles $h'(\eta)$, the temperature of the fluid $s(\eta)$ and temperature of dust particles $g(\eta)$ are illustrated below. At $\eta = 0$, the fluid transfers momentum to the dust particles in the early stage, causing the dust particles to move faster than the fluid. Since this study considered flow past an impulsively started sphere at $t = 0$, the boundary layer begins to develop, and the velocity increases as momentum is transferred. Over time, the velocity profile evolves as a function of time, influencing the boundary layer growth. Then, the applied magnetic field is assumed to be perpendicular to the fluid flow. According to the right-hand rule, the interaction between the magnetic field and fluid motion generates the Lorentz force, which accelerates the fluid in the direction of motion. To study the effects of M is varied incrementally from 0 to 1 in steps of 0.5. As M rises, $f'(\eta)$ and $h'(\eta)$ rises, as illustrated in Figure 4. The presence of the Lorentz force enhances fluid velocity while reducing the momentum boundary layer thickness.

Based on the boundary conditions, the fluid flow starts from zero velocity and accelerates to a velocity of one. This boundary condition represents an increase in the fluid's momentum. According to the governing equations, the velocities of both the fluid and dust particles are directly proportional to the magnetic parameter. Therefore, as the magnetic parameter increases, the velocities of the fluid and dust particles also increase, resulting in a reduction of the boundary layer thickness for both phases. This behavior is consistent with the findings of Mohammad et al. [19]. Conversely, Izani and Ali [9] studied a flow where the velocity decreases from one to zero along a sheet, yet observed a similar trend in which the thickness of the boundary layer decreases as the magnetic parameter increases.

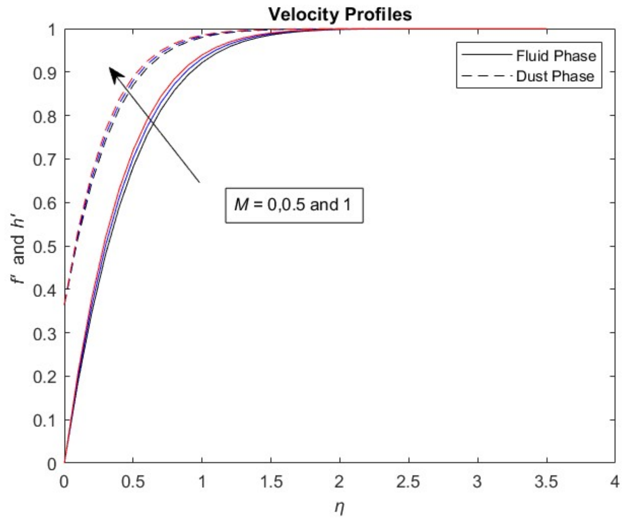

Figure 4: Velocity distribution for different value of $M = 0.0, 0.5$ and 1.0 showing that increasing M enhances the momentum of fluid and dust particles.

In Figure 5, the temperature profiles of $s(\eta)$ and $g(\eta)$ show a decreasing trend as M increases. The increase in velocity enhances convective effects, reducing heat transfer from the sphere's surface to the surrounding fluid and dust particles. Thus, both the fluid and dust particle temperatures gradually drop, approaching the boundary condition, leading to a thinner thermal boundary layer.

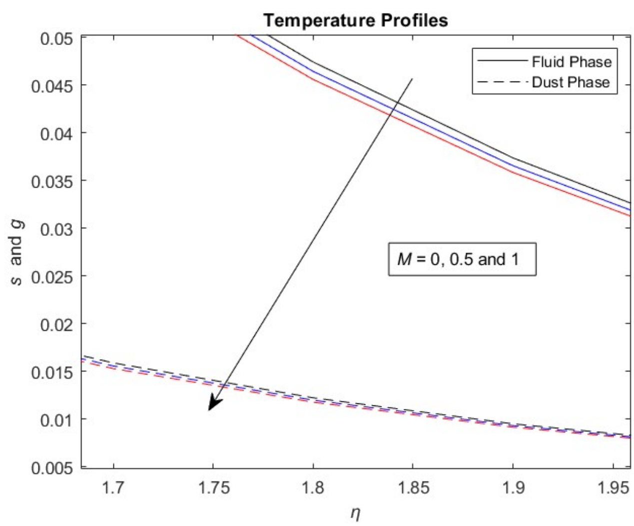

Figure 5: Temperature distribution for different value of $M = 0, 0.5$ and 1 showing that increasing M reduces the thermal energy of both fluid and dust particles

Figures 6 and 7 illustrate the velocity and temperature profiles concerning dust particle mass concentration G . As shown in Figure 4, an increase in G results in higher velocities for both the fluid $f'(\eta)$ and dust particles $h'(\eta)$. Initially, G is set to 1 to represent the adequate value to effectively represent of dust particles in the fluid flow 2, [9]. A higher value, $G = 5$, corresponds to a greater concentration of dust particles within the fluid. As increases, the dust particles contribute to momentum transfer, enhancing the overall velocity of the fluid. Despite their small size, their increased concentration significantly influences the flow behavior. The rise in velocity leads to stronger convective effects, which in turn enhance heat dissipation, causing $s(\eta)$ and $g(\eta)$ to decrease, as illustrated in Figure 7.

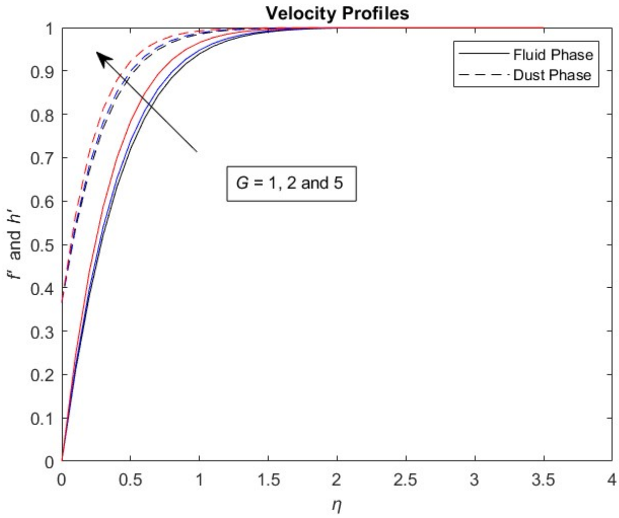

Figure 6: Velocity distribution for different value of $G = 1, 2$ and 5 showing that increasing G enhances the momentum of fluid and dust particles

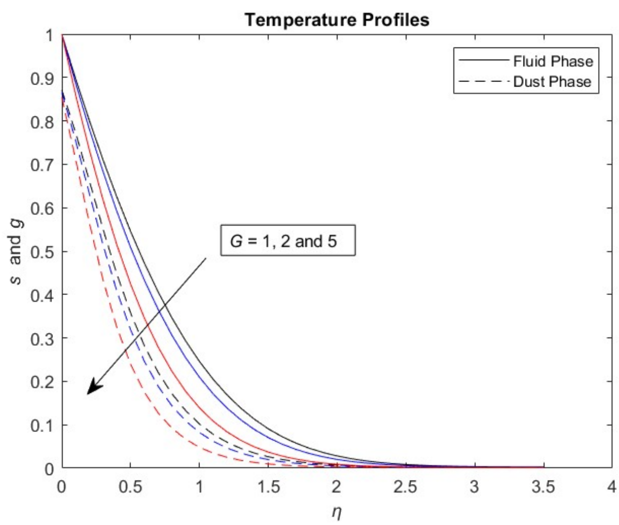

Figure 7: Temperature distribution for different value of $G = 1.0, 2.0$ and 5.0 showing that increasing G reduces the momentum of fluid and dust particles.

Figure 8 illustrates that increasing of β_v influences the velocity of both phases, with momentum transfer enhancing $h'(\eta)$ while limiting the increase of $f'(\eta)$. To analyze this effect, the fluid-particle interaction parameter and specific heat ratio are increased by 0.5, allowing for a systematic observation of parameter variations. This interaction quantifies the extent of momentum transfer between the fluid and dust particles. Initially, as the flow begins, the driven velocity transfers momentum to the densely distributed dust particles within the fluid. As shown in Figure 8, $f'(\eta)$ does not significantly increase due to the substantial momentum transfer to the dust particles. This causes the dust particles to move faster than the fluid. Over time, they act as momentum carriers, transferring energy until they reach a relaxation state, where their velocity stabilizes relative to the surrounding fluid. Since momentum and thermal energy are interconnected in fluid flow, a similar trend is observed in temperature behavior. As depicted in Figure 9, the fluid and dust particles exchange heat until they reach thermal equilibrium.

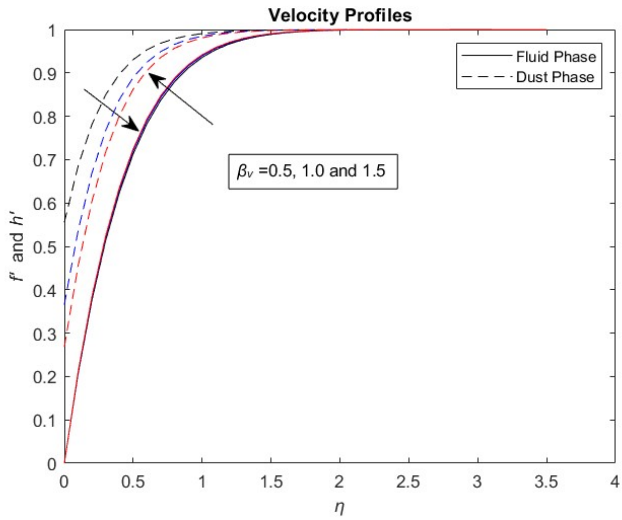

Figure 8: Velocity distribution for different value of $\beta_v = 0.5, 1.0$ and 1.5 showing that increasing β_v parameter enhances fluid momentum while reducing the momentum of dust particles.

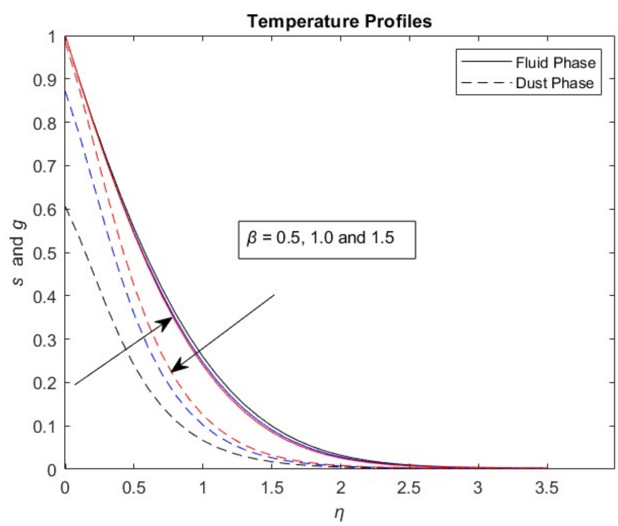

Figure 9: Temperature distribution for different value of $\beta_T = 0.5, 1.0$ and 1.5 showing that increasing β_T parameter reduces the fluid thermal energy while enhancing the thermal response of dust particles due to energy mechanisms.

Figure 10 illustrates the temperature distribution of the fluid and dust particles concerning variations in the specific heat ratio, γ. Since γ represents the ratio of dust particle heat capacity, c_p to fluid heat capacity, c_f, an increase in γ proportionally raises the specific heat of the dust particles. A higher specific heat ratio corresponds to a lower heat transfer rate between the sphere's surface to the fluid, and the dust particles. As a result, $s(\eta)$ and $g(\eta)$ experience a drop in temperature due to reduced heat transfer, as illustrated in Figure 10.

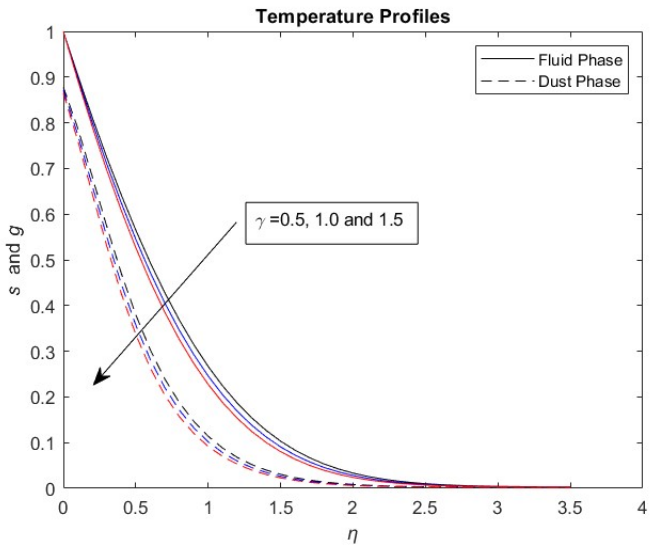

Figure 10: Temperature distribution for different value of $\gamma = 0.5$, 1.0 and 1.5 showing that increasing γ parameter reduces the thermal energy of both fluid and dust particles.

Table 2 presents the observed effects of various parameters in this study. When M and G increase, both the fluid and dust phases follow a similar trend-velocity increases while temperature decreases. However, the influence of β_v, β_T and γ is the opposite, meaning an increase in these parameters contributes to a decline in velocity and an increase in temperature for both phases. This indicates that the magnetic field and dust particle density enhance the fluid's momentum while reducing its temperature. This occurs because a stronger magnetic field generates Lorentz forces that accelerate fluid motion, while increased dust density facilitates momentum transfer but reduces thermal energy dissipation.

Table 2: Behavior of different parameters for velocity and temperature profiles at $t = 1.5$ and Pr$= 0.7$.

M	G	β_v	β_T	γ	$f'(\eta)$	$h'(\eta)$	s	g
0.0 0.5 1.0	1.0	1.0	1.0	1.0	$\uparrow$	$\uparrow$	$\downarrow$	$\downarrow$
1.0	1.0 2.0 5.0	1.0	1.0	1.0	$\uparrow$	$\uparrow$	$\uparrow$	$\downarrow$
1.0	1.0	0.5 1.0 1.5	1.0	1.0	$\uparrow$	$\downarrow$	–	–
1.0	1.0	1.0	0.5 1.0 1.5	1.0	–	–	$\downarrow$	$\uparrow$
1.0	1.0	1.0	1.0	0.5 1.0 1.5	–	–	$\downarrow$	$\downarrow$

5 Conclusions

This study presents a novel investigation into the unsteady magnetohydrodynamic(MHD) boundary layer flow of a dusty fluid over a sphere, emphasizing the coupled effects of magnetic fields, dust particle behavior, and heat transfer in a two-phase system. Unlike prior works that primarily focus on steady or single-phase flows, this research incorporates unsteady dynamics and particle-fluid interactions over a spherical geometry, enhancing the understanding of such complex flows.

The results demonstrate that increasing magnetic field strength and dust concentration significantly enhances fluid velocity while reducing temperatures in both fluid and dust phases. This is attributed to the Lorentz force accelerating the flow and promoting convective heat transfer. Additionally, stronger magnetic and dust effects reduce the thickness of momentum and thermal boundary layers by enhancing momentum exchange between phases. Over time, velocity and temperature stabilize as the two phases approach mechanical and thermal equilibrium. The thermal response is further influenced by the specific heat capacities of the dust and fluid, with a higher dust heat capacity facilitating greater heat absorption.

In this study, it is assumed that by employing nondimensionalization, physical units are removed, which simplifies the mathematical model and reduces the number of governing variables. This assumption enhances the generality and adaptability of the results to various fluid systems and improves computational efficiency. Moreover, the use of dimensionless parameters and similarity transformations is assumed to provide clearer physical insight into the flow behavior and heat transfer processes, thereby broadening the practical applicability of the findings.

A limitation of this study is that the analysis focuses solely on the forward stagnation point rather than examining flow along the entire surface of the sphere. As a result, a complete characterization of skin friction and Nusselt number distributions is not achieved. Additionally, this work considers only heat transfer effects and does not incorporate mass transfer, which limits the scope of the convective transport phenomena addressed.

Future investigations could enhance the model by exploring flow characteristics across the entire spherical surface rather than only at the stagnation point, offering a more thorough insight into dusty fluid flow. Additionally, incorporating the Coriolis force would enable analysis of rotating systems, which is important for understanding environmental phenomena such as haze formation that involve magnetic interactions with dust particles.

Acknowledgement This study is entirely funded by Universiti Teknologi Malaysia (UTM) Nexus, providing essential support to ensure its feasibility and effectiveness.

Conflicts of Interest The authors declare no conflict of interest.

References

[1] F. Ali, G. Ali, A. Khan, I. Khan, E. T. Eldin & M. Ahmad (2023). Effects of newtonian heating and heat generation on magnetohydrodynamics dusty fluid flow between two parallel plates. *Frontiers in Materials*, *10*(1), Article ID: 1120963. https://doi.org/10.3389/fmats.2023.1120963.

[2] M. Athar, A. Ahmad & Y. Khan (2023). Polymer presence in boundary layer flow and heat transfer of dusty fluid over a stretching surface. *Multidiscipline Modeling in Materials and Structures*, *19*(4), 617–633. https://doi.org/10.1108/MMMS-09-2022-0167.

[3] T. Aurégan, T. Bonometti & J. Magnaudet (2023). Flow past a sphere translating along the axis of a rotating fluid: Revisiting numerically Maxworthy's experiments. *Journal of Fluid Mechanics*, *967*, Article ID: A25. https://doi.org/10.1017/jfm.2023.469.

[4] A. J. Chamkha & S. E. Ahmed (2012). Unsteady MHD heat and mass transfer by mixed convection flow in the forward stagnation region of a rotating sphere at different wall conditions. *Chemical Engineering Communications*, *199*(1), 122–141. https://doi.org/10.1080/00986445.2011.575907.

[5] M. Chitra, R. Bhaskaran & S. Parthasarathy (2018). Effects of oscillatory motion of a viscoelastic dusty fluid (blood) through arteries under the influence of magnetic field with porous medium. In *Journal of Physics: Conference Series, International Conference on Applied and Computational Mathematics 10 August 2018, Tamilnadu, India*, volume 1139 pp. Article ID: 012004. IOP Publishing, Bristol. https://doi.org/10.1088/1742-6596/1139/1/012004.

[6] A. Dawar & N. Acharya (2022). Unsteady mixed convective radiative nanofluid flow in the stagnation point region of a revolving sphere considering the influence of nanoparticles diameter and nanolayer. *Journal of the Indian Chemical Society*, *99*(10), Article ID: 100716. https://doi.org/10.1016/j.jics.2022.100716.

[7] X. Y. Gao, Y. J. Guo & W. R. Shan (2023). Theoretical investigations on a variable-coefficient generalized forced–perturbed Korteweg–de Vries–Burgers model for a dilated artery, blood vessel or circulatory system with experimental support. *Communications in Theoretical Physics*, *75*(11), Article ID: 115006. https://doi.org/10.1088/1572-9494/acbf24.

[8] F. Henrique & F. R. Cunha (2025). Dispersion and particle pressure in sedimenting suspensions with hydrodynamic interactions and particle inertia. *International Journal of Multiphase Flow*, *182*, Article ID: 105037. https://doi.org/10.1016/j.ijmultiphaseflow.2024.105037.

[9] S. N. H. Izani & A. Ali (2019). Thermal radiation effects on heat and mass transfer of magnetohydrodynamics dusty Jeffrey fluid past an exponentially stretching sheet. *Matematika*, *35*(2), 187–200. https://doi.org/10.11113/matematika.v35.n2.1172.

[10] S. Jaffrullah, W. Sridhar & G. R. Ganesh (2024). Analysis of MHD Casson nanofluid flow over a nonlinearly stretching surface with joule heating, radiation and suction effects. *International Journal of Heat & Technology*, *42*(2), 414–426. https://doi.org/10.18280/ijht.420207.

[11] N. N. N. Jefri & A. Ali (2024). Unsteady dusty MHD boundary layer flow past a sphere. In *ITM Web of Conferences: The 19th IMT-GT International Conference on Mathematics, Statistics and Their Applications (ICMSA 2024)*, volume 67 pp. Article ID: 01030. EDP Sciences, Les Ulis, France. https://doi.org/10.1051/itmconf/20246701030.

[12] N. N. N. Jefri & A. Ali (2025). Separation points analysis on unsteady MHD mixed convective heat transfer past a sphere in Casson fluid. *Malaysian Journal of Mathematical Sciences*, *19*(4), 1417–1436. https://doi.org/10.47836/mjms.19.4.13.

[13] K. L. J. Kan, K. W. E. Cheng & H. C. Zhuang (2023). Electric analysis of the maritime application high-frequency magnetohydrodynamic thruster. *Energies*, *16*(16), Article ID: 6021. https://doi.org/10.3390/en16166021.

[14] A. R. M. Kasim, N. S. Arifin, N. A. N. Ariffin, M. Z. Salleh & M. I. Anwar (2020). Mathematical model of simultaneous flow between Casson fluid and dust particle over a vertical stretching sheet. *International Journal of Integrated Engineering*, *12*(3), 253–260. https://doi.org/10.30880/ijie.2020.12.03.029.

[15] N. S. Khan, A. H. Usman, A. Kaewkhao, P. Kumam, P. Thounthong & U. W. Humphries (2021). Exploring the nanomechanical concepts of development through recent updates in magnetically guided system. *Scientific Reports*, *11*(1), Article ID: 13576. https://doi.org/10.1038/s41598-021-92440-4.

[16] A. Kumar, P. Sethy, A. K. Ray & A. Kumari (2025). Mixed convection magnetohydrodynamic flow of hybrid nanofluid over a spinning sphere with nonlinear thermal radiation: Keller-Box approach. *Numerical Heat Transfer, Part A: Applications*, *86*(7), 1983–2009. https://doi.org/10.1080/10407782.2023.2285358.

[17] A. Mahdy & H. A. Nabwey (2020). Microorganisms time-mixed convection nanofluid flow by the stagnation domain of an impulsively rotating sphere due to Newtonian heating. *Results in Physics*, *19*, Article ID: 103347. https://doi.org/10.1016/j.rinp.2020.103347.

[18] A. E. N. Mahdy, F. M. Hady & H. A. Nabwey (2021). Unsteady homogeneous-heterogeneous reactions in MHD nanofluid mixed convection flow past a stagnation point of an impulsively rotating sphere. *Thermal Science*, *25*(1 Part A), 243–256. https://doi.org/10.2298/TSCI190712388M.

[19] N. F. Mohammad, A. R. M. Kasim, A. Ali & S. Shafie (2014). Separation times analysis of unsteady magnetohydrodynamics mixed convective flow past a sphere. In *AIP Conference Proceedings: Proceedings of The 21st National Symposium on Mathematical Sciences (SKSM21): Germination of Mathematical Sciences Education and Research Towards Global Sustainability, 6–8 November 2013, Penang, Malaysia*, volume 1605 pp. 349–354. American Institute of Physics, College Park, Maryland. https://doi.org/10.1063/1.4887614.

[20] C. Pandey & B. R. Kumar (2023). A numerical method for MHD Stokes model with applications in blood flow. *Computational and Mathematical Biophysics*, *11*(1), Article ID: 20230105. https://doi.org/10.1515/cmb-2023-0105.

[21] J. Rajakumar, P. Saikrishnan & A. Chamkha (2016). Non-uniform mass transfer in MHD mixed convection flow of water over a sphere with variable viscosity and Prandtl number. *International Journal of Numerical Methods for Heat & Fluid Flow*, *26*(7), 2235–2251. https://doi.org/10.1108/HFF-05-2015-0189.

[22] B. H. S. Raju, D. Nath, S. Pati & L. Baranyi (2020). Analysis of mixed convective heat transfer from a sphere with an aligned magnetic field. *International Journal of Heat and Mass Transfer*, *162*, Article ID: 120342. https://doi.org/10.1016/j.ijheatmasstransfer.2020.120342.

[23] C. Q. Ru (2024). Stability of plane parallel flow revisited for particle–fluid suspensions. *Journal of Applied Mechanics*, *91*(11), Article ID: 111005. https://doi.org/10.1115/1.4066089.

[24] K. Sajjan, M. Dinesh Kumar, C. Raju, S. M. Upadhya & S. N (2025). Exploration of uniform and sudden lifting on hybrid nanofluid flow induced by the ramped motion of magnetized porous plate suspended by dust particles. *Numerical Heat Transfer, Part A: Applications*, *86*(20), 7373–7391. https://doi.org/10.1080/10407782.2024.2350038.

[25] K. M. Satwai N. Prasad & M. V. Phani Kumari (2025). Analysis of blood flow with nanoparticles through a porous inclined overlapping stenosed artery under the influence of external magnetic field. *Malaysian Journal of Mathematical Sciences*, *19*(3), 767–787. https://https://doi.org/10.47836/mjms.19.3.01.

[26] W. Sridhar, G. Dharmaiah, K. AL-Farhany & M. F. Al-Dawody (2024). A computational ascertainment of Hall and ion slip implications over a stretched regime with chemical reaction and internal heat source. *International Journal of Ambient Energy*, *45*(1), Article ID: 2288145. https://doi.org/10.1080/01430750.2023.2288145.

[27] B. Widodo, Y. Norasia & D. Adzkiya (2019). MHD fluid flow with the effect of mixed convection passing on a magnetic sphere in Newtonian nano fluid. In *Journal of Physics: Conference Series: International Conference on Mathematics: Pure, Applied and Computation 20 October 2018, Surabaya, Indonesia*, volume 1218 pp. Article ID: 012057. IOP Publishing, Bristol. https://doi.org/10.1088/1742-6596/1218.